Proceedings of the ASME 2025
International Design Engineering Technical Conferences &
Computers and Information in Engineering Conference
IDETC/CIE2025
August 17-20, 2025, Anahiem, California, USA

DETC2025-XXXXX

A MULTIDISCIPLINARY DESIGN OPTIMIZATION FRAMEWORK FOR WAVE-DRIVEN DESALINATION SYSTEMS

Nate DeGoede[1]*, **Maha Haji**[1]
[1]Sibley School of Mechanical and Aerospace Engineering
Cornell University
Ithaca, New York 14853
Email: {njd76, maha}@cornell.edu

ABSTRACT

Seawater reverse osmosis (SWRO) desalination offers a critical solution to global water scarcity, but its high energy demand necessitates sustainable power sources. Wave energy converters (WECs) present a promising alternative, particularly wave-driven desalination systems (WDDS), where they directly pressurize seawater without the inefficiencies of electrical conversion. Despite this potential, high costs remain a barrier to widespread adoption.

This study introduces a multidisciplinary design optimization (MDO) framework to enhance WDDS performance and cost-effectiveness. The framework integrates hydrodynamics, system dynamics, desalination processes, and economic modeling, enabling holistic system-level optimization. As a precursor to full MDO, a Latin hypercube sampling (LHS) design of experiments (DOE) study is conducted to explore key design trade-offs.

Results highlight the importance of balancing WEC, power take-off (PTO), and desalination plant sizing. Notably, traditional designs favoring large accumulators and small SWRO plants may benefit from smaller accumulators and increased SWRO plant capacity, reducing the levelized cost of water (LCOW). Feature importance analysis further identifies key parameters influencing performance, guiding future optimization. Optimization results are forthcoming and will be included in the final paper and presentation.

This study lays the groundwork for cost-effective WDDS development, demonstrating the potential of MDO methodologies to improve desalination affordability and sustainability.

1 Introduction

The world is facing a growing water crisis, with global freshwater demand projected to grow over 40% by 2050 [1]. This rising demand, compounded by factors such as droughts, urbanization, and uneven distribution of water resources, will put immense stress on existing freshwater supplies. Seawater reverse osmosis (SWRO) is promising solution to mitigate this stress by providing desalinated water. However, SWRO is energy-intensive, requiring 2-4 kWh/m^3 [2]. If powered by fossil fuels, this process would further contribute to climate change, exacerbating water scarcity issues [3]. Therefore, to ensure sustainability, SWRO must be powered by renewable energy sources.

Wave Energy Converters (WECs) offer a compelling solution. Both SWRO and WECs are marine-based technologies, with SWRO plants typically located on the coast and WECs deployed offshore. Beyond this natural co-location, WECs are particularly suited for SWRO [4] due to their ability to directly pressurize seawater using a hydraulic style power take-off (PTO) system, forming a wave-driven desalination system (WDDS) [5]. Unlike other renewable energy sources that require energy conversion to electricity, WECs can provide direct mechanical power, improving overall efficiency.

Despite their potential, WECs face significant economic and technical challenges, with high costs being a primary barrier to widespread adoption. Design optimization is therefore es-

*Corresponding Author

sential for reducing costs and improving performance. Multidisciplinary Design Optimization (MDO) provides a systematic framework for addressing these challenges by integrating multiple interdependent subsystems into a unified design process, allowing for global optimization rather than isolated improvements [6]. MDO-style approaches integrating PTO design with hydrodynamics and/or controls have successfully enhanced electricity-generating WECs, demonstrating its potential to enhance efficiency and energy output [7, 8, 9, 10]. For instance, Michelén Ströfer et al. (2023) achieved a 22% increase in electrical power output using control co-design (CCD), while Grasberger et al. (2024) demonstrated a 60% improvement in normalized power output compared to traditional sequential design methods. These studies emphasize the importance of holistic modeling, which accounts for wave dynamics, WEC operation, PTO performance, and control strategies. Although these studies have showed great promise for MDO to improve WECs, these approaches have yet to be applied to WDDS, leaving a critical gap in research.

This study addresses this gap by developing a holistic MDO framework for WDDS. As a precursor to full optimization, a design of experiments (DOE) study is conducted to explore key system parameters and establish a foundation for optimizing freshwater production. A simplified WDDS architecture is introduced (Fig 1), where an oscillating surge wave energy converter (OSWEC) drives a piston pump, pressurizing seawater and delivering it to an onshore SWRO plant. The high-pressure seawater enables freshwater production without requiring external energy input. While similar systems have been studied [11, 12, 13, 14], this study excludes an energy recovery unit (ERU)—a component known to enhance efficiency—to focus on the MDO aspects of the system. A comparison between configurations with and without the ERU will be the topic of future work.

The concept sketch in Fig 1 provides an overview of the WDDS but does not depict all hydraulic components included in this study. Key elements such as the hydraulic accumulator, pressure relief valve, brine side throttle valve, and directional control valves are omitted for simplicity. A detailed hydraulic

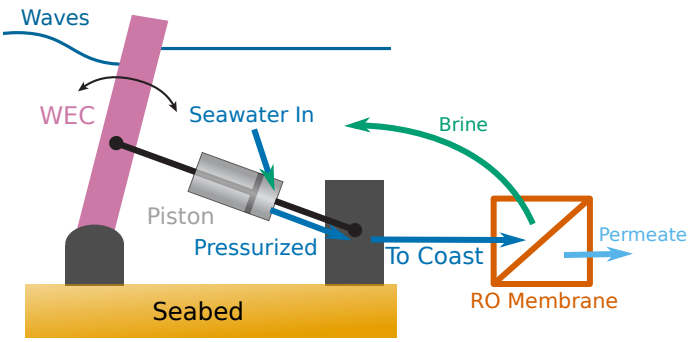

FIGURE 1: Simple wave-driven desalination system (WDDS) concept Sketch.

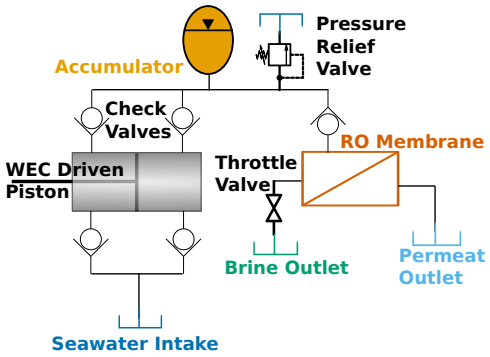

FIGURE 2: Hydraulic circuit diagram of the WDDS.

circuit diagram, including these components, is show in Fig 2.

The following sections present the MDO problem formulation, defining the design variables that shape the design space. A comprehensive WDDS model is then introduced, structured into key modules: desalination plant, hydrodynamics, system dynamics, and economic analysis. Finally a DOE is conducted to illustrate the potential design insights that full optimization could provide. Full optimization results are forthcoming and will be included in the final paper and presented at the conference.

All code for this study can be accessed at https://github.com/symbiotic-engineering/mdo_wd2.

2 Problem Formulation

2.1 Multidisciplinary Design Optimization Framework

The optimization problem in this study is formally defined as:

$$\begin{aligned} \text{Minimize} \quad & \text{LCOW}(\mathbf{x}, \mathbf{p}; \hat{u}) \\ \text{by varying} \quad & \mathbf{x} \\ \text{subject to} \quad & \mathbf{g} \leq 0 \\ & \mathbf{h} = 0 \\ \text{while solving} \quad & \mathbf{R}(\mathbf{x}, \mathbf{p}; \hat{u}) = 0 \\ \text{for} \quad & \hat{u} \end{aligned}$$

where LCOW (levelized cost of water) is the objective function to be minimized (further discussed in section 3.4), $\mathbf{x}$ represents a vector of design variables, $\mathbf{p}$ represents a vector of parameters, and $\hat{u}$ is the vector of coupled variables. The constraints include inequality constraints ($\mathbf{g} \leq 0$) and equality constraints ($\mathbf{h} = 0$), while $\mathbf{R}$ represents the governing equations for different disciplinary modules. The different disciplines represented in this framework are seawater desalination, hydrodynamics, system dynamics, and economics, and are discussed further in the system modeling section (Section 3). Controls are not included at this time, but will be included in future work.

2.2 Design Space

The design vector, $\mathbf{x}$, consists of the following variables: WEC width, w [m], WEC thickness, t [m], WEC mass, m [kg], the distance from the WEC hinge to the PTO joint, ℓ_1 [m], piston area, A_p [m^2], accumulator volume, V_{acc} [m^3], accumulator pre-charge pressure, P_0 [MPa], and SWRO plant capacity, $Q_{p,max}$ [m^3/day]. Table 1 summarizes the design variables, their bounds and nominal values. Some of the key WEC dimensions are shown in Fig. 3.

TABLE 1: Design variables

Variable	Nominal Value	Lower Bound	Upper Bound
w	18 m	10 m	30 m
t	2 m	1 m	5 m
m	127×10^3 kg	50×10^3 kg	500×10^3 kg
ℓ_1	2 m	0.1 m	draft
A_p	0.26 m^2	0.01 m^2	1 m^2
V_{acc}	4 m^3	0.01 m^3	6 m^3
P_0	3 MPa	1 MPa	7 MPa
$Q_{p,max}$	3150 m^3/day	1000 m^3/day	10000 m^3/day

One notable aspect of the bounds is that the upper bound of ℓ_1 is set to the draft parameter rather than a fixed value. The draft represents the distance from the still water line to the bottom of the WEC float. The WEC width refers to the sway dimension, while the WEC thickness corresponds to the surge dimension. To reduce the dimensionality of the design space, draft and height are excluded as design variables, as the chosen variables already provide sufficient control WEC dynamics. The WEC dimensions are illustrated in Fig. 3. Additionally, to aid in the interpretation of ℓ_1, a mechanism diagram is provided in Fig. 4, which also shows the intakes location defined by ℓ_2 and ℓ_3 (both of which are parameters rather than design variables).

2.3 Parameters and Constraints

Parameters were largely reflect the parameters used by Yu and Jenne (2018) [11]. The subcategories of parameters include: general (parameters like gravity and wave conditions), desalination, WEC, mechanism, and solver parameters for the different submodules. Full tables of parameters can be found in appendix A.

Constraints are largely enforced by the system dynamics module (Section 3.3). These constraints are applied to constrain

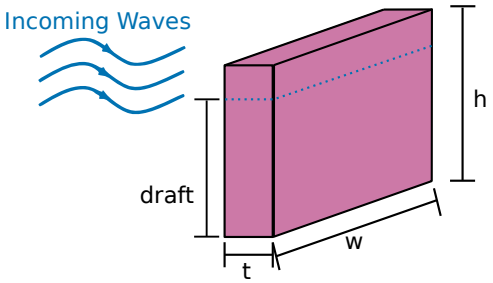

FIGURE 3: WEC Dimensions. Note that h represents the WEC height, which is a parameter rather than a design variable.

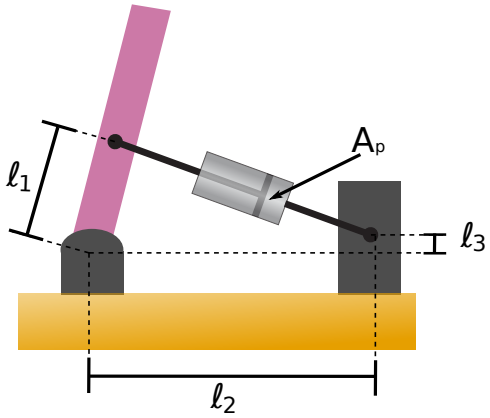

FIGURE 4: Mechanism Diagram.

piston motion, ensure SWRO plant is not operated above capacity, and to ensure force and energy balance within the system.

2.4 Optimization Algorithm

A genetic algorithm (GA) is the most suitable choice for this problem due to the absence of accessible gradients in the hydrodynamics (Section 3.2) and system dynamics (Section 3.3) modules. While finite differencing these modules is theoretically possible, these modules are highly computationally expensive, making such an approach impractical. Consequently, a heuristic algorithm like a GA is the best choice. Optimization results are forthcoming and will be included in the final paper and presented at the conference.

3 System Modeling

The system model is depicted in the N^2 Diagram in Fig. 5, illustrating the relationships between different disciplinary modules. Arrows represent data flow between modules, showing interdependence across the system. The model consists of four primary modules: “Desal”, which calculates dependent variables related to the SWRO plant, “Hydro”, which calculates depen-

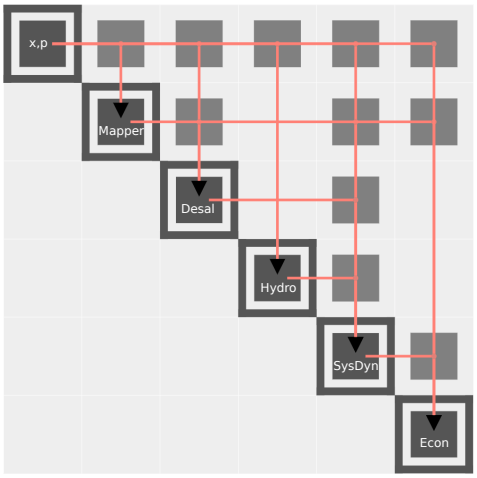

FIGURE 5: N^2 Diagram of the WDDS System Model.

dent variables related to the wave-structure interaction, "SysDyn" which solves the system dynamics of the WDDS, and "Econ" which evaluates the LCOW objective. Additionally, a "Mapper" module is included to map variables and parameters to dependent variables across different modules. However, since it does not contribute to independent disciplinary calculations, it is not considered a separate discipline. The four main modules are discussed in more detail in the following subsections.

3.1 Desalination Module

The desalination module calculates key parameters for the SWRO plant, considering the system's capacity and seawater composition. The reverse osmosis process is governed by:

$$Q_p = A_w A_m (\Delta P - \Delta\pi) \tag{1}$$

where Q_p [m^3/s] is the permeate flow rate, A_w [m^2] is the water permeability coefficient, A_m [m^2] is the membrane area, ΔP [Pa] is the pressure difference across the membrane, and $\Delta\pi$ [Pa] is the osmotic pressure difference across the membrane. The osmotic pressure is calculated using [15]:

$$\pi = iCRT \tag{2}$$

where i [-] is the number of ions produced per molecule of solute, C [mol/m^3] is the concentration of the solute, R [J/K-mol] is the ideal gas constant, and T [K] is the temperature.

For seawater applications, Applegate's empirical formula [15] provides an alternative method for calculating osmotic pressure:

$$\pi = 1.12T\sum m_i \tag{3}$$

where $\sum m_i$ [mol/m^3] represents the sum of dissolved ion molarities. In this study, we use Eq. 2 as our primary method. Eq. 3 is provided as an alternative where precise seawater composition data is available. In this study, we set $\Delta\pi$ to the osmotic pressure of the seawater minus the target permeate osmotic pressure.

For the water permeability coefficient (A_w) we adopt the constant value of 2.57×10^{-12} m^3/N-s, as reported by Yu and Jenne (2018) [11]. This choice is justified by our use of the same SWRO membrane, the SW30HR-380 Dry from DuPont [16], for which their coefficient was determined. The membrane area A_m is then given by

$$A_m = \frac{Q_{p,max}}{Q_0} A_0 \tag{4}$$

where Q_0 and A_0 are the nominal flow rate and membrane area for the SW30HR-380 membrane, found on the datasheet [16].

At this stage, Eq. 1 relates only pressure and flow rate. To integrate this relationship into system dynamics, we define the membrane resistance (R_m [MPa-s/m^3]) as:

$$\frac{1}{A_w A_m} \tag{5}$$

This allows for a linearized resistance model, simplifying system-level calculations.

To avoid running the system above capacity, a pressure relief valve is included, with its set pressure P_{relief} [MPa] defined as:

$$P_{\text{relief}} = Q_{p,max} R_m + \Delta\pi \tag{6}$$

This equation ensures that if the flow exceeds the system's capacity, the pressure relief valve will open. Notably, by combining Eqs. 4 5 and 6, the dependency on $Q_{p,max}$ cancels out, making P_{relief} independent of specific design parameters under the current membrane resistance model. However, this remains a dependent variable, allowing for flexibility in alternative design spaces or resistance models.

For flow to pass through the membrane, resistance on the brine side is required. This can achieved using a throttle valve (as modeled in this study), or an ERU (for higher efficiency in advanced designs). In this study we implement a constant throttle valve resistance (R_t [MPa-s/m^3]), calculated such that when the system runs at full capacity, it also runs at the recommended recovery ratio, η_{RO}, given the SW30HR-380 membrane and the specified seawater composition.

$$R_t = \frac{P_{\text{relief}}}{Q_{p,max}(\frac{1}{\eta_{RO}} - 1)} \tag{7}$$

3.2 Hydrodynamics

Starting from Newton's second law, Falnes and Kurniawan (2022) [17] define the equation of motion for an oscillating WEC as:

$$I\ddot{\xi} = f_e - f_r - f_b - f_v - f_f - f_u \tag{8}$$

where I [m or kg-m^2] is the inertia of the WEC, dependent on WEC mass m (a design variable), ξ [m or rad] is the body linear or angular motion, f_e [N or Nm] is the excitation force or torque due to incident waves, f_r [N or Nm] is the radiation force or torque due to the WEC's oscillations, accounting for added mass and radiation damping, f_b [N or Nm] is the hydrostatic force or torque due to buoyancy and restoring effects, f_v [N or Nm] is the drag force or torque which arises from nonlinear viscous effects (neglected in this study), f_f [N or Nm] is the force or torque that captures friction forces (also neglected), and f_u [N or Nm] is the PTO force or torque, which represents energy extraction by the WEC's power conversion system. The PTO force is modeled in the system dynamics module, while drag and friction are omitted, assuming linear potential flow theory. These simplifications are also made by Grasberger et al. (2024) [10] in their OSWEC study.

The hydrostatic force, which accounts for the buoyancy of the WEC and its tendency to return to equilibrium, is given by:

$$f_{hs} = K_{hs}\xi \tag{9}$$

where K_{hs} is the hydrostatic stiffness matrix.

The radiation force, which accounts for the radiated waves generated by the WEC motion, is expressed as:

$$f_r = A(\omega)\ddot{\xi} + B(\omega)\dot{\xi} \tag{10}$$

where $A(\omega)$ and $B(\omega)$ are the added mass and radiation damping matrices, respectively.

This formulation simplifies the WEC hydrodynamics to four key components: the excitation force, hydrostatic stiffness matrix, added mass matrix, and radiation damping matrix. These coefficients are computed using the open-source Boundary Element Method (BEM) solver Capytaine [18]. BEM solvers are well suited for wave-structure interaction problems as they only require meshing of the structure-fluid boundary, unlike traditional computational fluid dynamics (CFD) solvers which require full fluid volume meshing, significantly reducing computational cost [19].

For this study, the WEC flap is approximated as a rectangular prism, restricted to pitch motion about its bottom hinge. Notably, added mass, radiation damping, and excitation force are all frequency-dependent.

3.3 System Dynamics

The WDDS system dynamics are modeled in MATLAB+Simulink, capturing the interactions between the WEC and PTO system. The following sections detail the modeling of each subsystem.

3.3.1 Wave Energy Converter The WEC dynamics are modeled using WEC-Sim [20], an open-source software developed by the National Renewable Energy Laboratory (NREL) and Sandia National Laboratories. Using hydrodynamic coefficients obtained from the hydrodynamics module, WEC-Sim simulates WEC system dynamics within a Simulink-based framework, enabling efficient analysis of wave-structure interactions and PTO performance. WEC-Sim offers significant advantages over other WEC simulation tools by operating in the time domain, allowing it to capture complex dynamics and nonlinearities that many alternative methods can only approximate. The WEC is modeled as a two body system, with the base fixed to the seafloor and the flap limited to a one degree of freedom (pitch). The WEC model also includes the mechanism to drive the piston. With the intake location, hinge location, and PTO joint location all defined according to Fig. 4. The block diagram used to model the WEC is shown in Fig. 6.

3.3.2 Power Take-Off The desalination hydraulic circuit (Fig 2) is modeled using the isothermal liquid domain from the Simscape fluids toolbox. This domain is specialized for modeling hydraulic systems, and is a good fit for modeling the dynamics of the hydraulic circuit presented. The high level Simscape PTO model is shown in Fig. 7.

From this high level view, we can see the main components of the hydraulic circuit. The "piston_cylinder" block contains the piston and directional valves, followed by the accumulator and

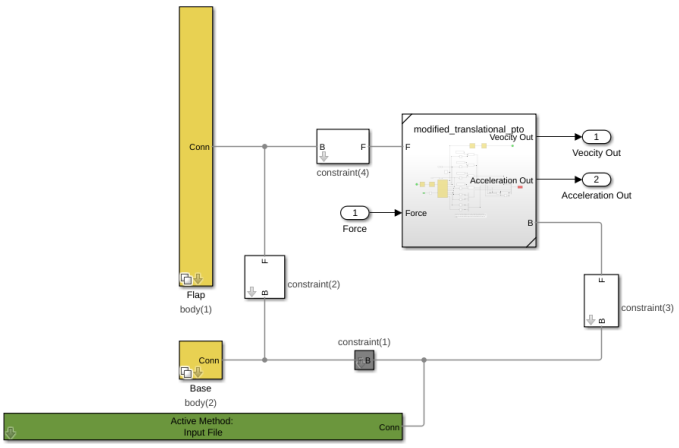

FIGURE 6: Model of the WEC in Simscape.

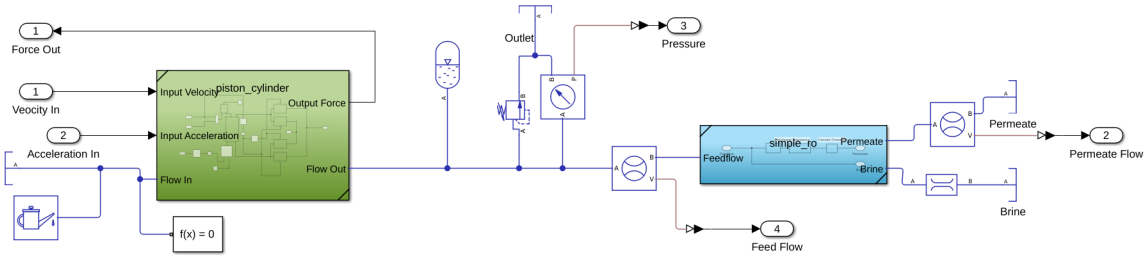

FIGURE 7: Model of the hydraulic circuit in Simscape.

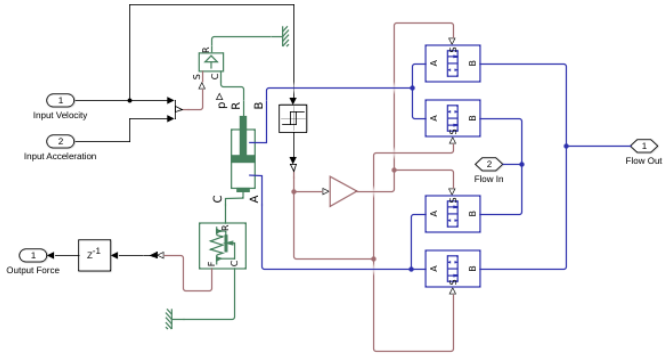

FIGURE 8: Model of the piston and directional valves in Simscape.

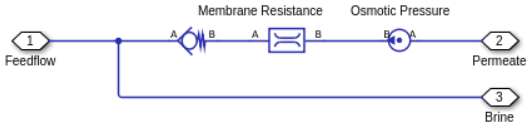

FIGURE 9: Model of the reverse osmosis membrane in Simscape.

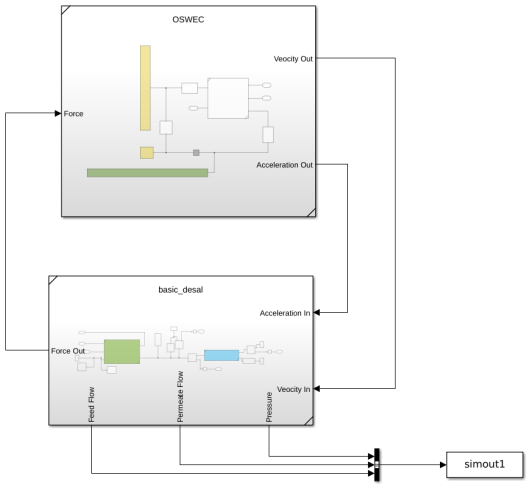

FIGURE 10: Model of the coupled WEC and PTO in Simscape.

pressure relief valve, as well as the reverse osmosis membrane, modeled in the "simple_ro" block, and finally the throttle valve on the brine side.

The "piston_cylinder" subsystem is further broken down in Fig. 8. This model features a single double-acting piston, though the system dynamics would remain largely unchanged if the piston area variable was distributed across multiple smaller pistons instead of a single large one. Another feature of note is the use of three-way controlled directional valves instead of check valves to simplify computations for the solver while maintaining the overall system dynamics.

The "simple_ro" subsystem is broken down in Fig. 9. This subsystem includes a check valve to prevent forward osmosis in low energy waves, followed by the membrane resistance and osmotic pressure blocks which allow for a Simscape representation of eq 1. The membrane resistance block is a linear resistance on the volumetric flow rate, and the osmotic pressure block applies a pressure on the permeate side equal to the osmotic pressure difference as calculated in eqns. 2 or 3.

3.3.3 Coupled Solver The two subsystems of the WEC and PTO are then coupled through as shown in Fig. 10. The velocity and acceleration signals are fed as inputs to the PTO from the WEC, and the force is fed back from the PTO to the WEC. WEC-Sim uses this coupled system to simulate the system dynamics of the WDDS. MATLAB's ode4 solver, a fourth order Runge-Kutta solver, with a 0.1 s time step is used to solve the system dynamics.

3.4 Economics

Our objective is to minimize the levelized cost of water (LCOW) [\$/m^3] which is calculated using the annual water production (AWP) [m^3/year] from the system dynamics module

and the costs calculated from the economic module. We consider a simple cost model comprised of two categories: capital (CAPEX) and operational expenditures (OPEX). The LCOW is then determined by

$$\text{LCOW} = \frac{(\text{FCR} \times \text{CAPEX}) + \text{OPEX}}{\text{AWP}} \tag{11}$$

where FCR is the fixed charge rate, 10.8% based on the assumptions made in the U.S. Department of Energy report [21]. We note that Eq. 11 takes a form similar to that of the levelized cost of energy (LCOE) used by the U.S. Department of Energy [21]. The CAPEX and OPEX are split into three sections based on the three main sections of design variables: the WEC, the PTO, and the desalination plant. It is important to note that this cost model is not meant to provide an exact representation of total system costs. Instead it serves as a tool to quantify relative cost savings between different designs, highlighting the impact of applying an MDO approach to this problem. An explanation of the cost model for each component is given below. Note that all costs are adjusted to 2025 USD.

3.4.1 Wave Energy Converter Cost modeling for WECs is inherently uncertain due to limited real world data, making it difficult to achieve high accuracy. This presents a significant challenge for studies like this, where levelized cost is used as an objective function. Despite these challenges, a practical and comparative cost model can still be developed to capture key cost trends and enable design comparisons. In this study, we follow the method from Grasberger et al. (2024) who introduced a simplified cost model for their OSWEC CCD study [10]. In this model, costs are expressed as a function of the float's surface area of the float through a combination of linear and logarithmic terms, shown below

$$\text{Cost} = C_{1,ref}\left(\frac{A_x}{A_{ref}}\right) + C_{2,ref}\left(1 + \log\left(\frac{A_x}{A_{ref}}\right)\right) \tag{12}$$

where A_x [m^2] is the surface area of the float, A_{ref} [m^2] is the surface area of the reference float, and $C_{1,ref}$ [\$] and $C_{2,ref}$ [\$] are the costs of the reference float associated with the two terms.The linear term captures cost associated with the structural components (the flap, base, and mooring), while the logarithmic term captures other expenses (PTO, monitoring, other OPEX) which are less dependent on the size of the float. This cost model relies on an accurate reference WEC for meaningful comparisons.

Given the importance of a reliable reference WEC, we utilize NREL's Reference Model 5 (RM5) [22], a well-documented OSWEC. Its similarity to the WEC design in this study makes it an appropriate benchmark for cost comparison and performance evaluation. To tailor the cost model to this study's specific WEC design, we exclude certain cost components that are not relevant or do not scale directly with WEC size. In particular, since this design replaces an electricity-generating PTO with the a SWRO PTO, the electrical PTO costs from the initial RM5 cost model are not include. Instead, we determine SWRO PTO specific costs, detailed in the next section. Additionally, because this study considers a nearshore fixed-bottom WEC, many mooring-related expenses from the reference RM5 are not included. Finally, many transit and other overhead design costs are excluded as they are unlikely to scale proportionally with the size of the WEC.

3.4.2 Power Take-Off The PTO cost model covers the costs associated with the pumping mechanism, the piston cylinder, and the accumulator. At present, pumping mechanism and piston cylinder costs are under development and are not included in this preliminary study. Despite this exclusion, we believe the current model offers important insights into the accumulator sizing. The accumulator cost is modeled as function of the accumulator volume (V_{acc}). The accumulator volume design variable is rounded up to the nearest standard size based on commercially available accumulators from Reasontek [23] (2.5 gallons). The accumulator volume is then split into the nominal sizes available and the required amount of each size is multiplied by the quoted cost of that size. A cost optimal accumulator configuration for a given volume is achieved when the volume is split into the as many 15 gallon accumulators as possible, followed by 10 gallon accumulators, then 5 gallon accumulators, and finally 2.5 gallon accumulators.

3.4.3 Desalination Plant The costs associated with the desalination plant are divided into two categories: capital costs and operational costs. The capital costs includes all expenses related to the construction and installation of the plant, while the operational costs over the recurring costs associated with its annual operation and maintenance.

Cost models for small- to mid-scale SWRO desalination plants of this scale (producing thousands of m^3/day) are scares and often poorly documented or inconsistently implemented. Most well-documented economic studies focus on large-scale plants (hundreds of thousands of m^3/day) [24, 25, 26, 27], making them less applicable to this study. Meanwhile, studies that examining smaller desalination plants frequently lack transparent methodologies for estimating SWRO-specific plant costs [28,29]. One notable study on wave-driven desalination employs the Desalination Economic Evaluation Program (DEEP 5.1) developed by the International Atomic Energy Agency to estimate unit CAPEX cost [30]. However, DEEP 5.1 itself is poorly documented [31], making it difficult to assess the accuracy and reliability of its cost estimates.

Given these limitations, this study adopts a cost estimation methodology based on the work of Voutckov in *Desalination*

TABLE 2: Designs with Minimum and Maximum LCOW

Variable	Min LCOW case	Max LCOW case
w	11.5 m	24.5 m
t	4.35 m	1.23 m
m	490 $\times 10^3$ kg	139 $\times 10^3$ kg
ℓ_1	3.11 m	0.276 m
A_p	0.932 m^2	0.394 m^2
V_{acc}	1.51 m^3	0.237 m^3
P_0	4.51 MPa	3.92 MPa
$Q_{p,max}$	7467 m^3/day	9681 m^3/day
LCOW	2.29 \$/m^3	7547 \$/m^3

Project Cost Estimating and Management [32]. Using the cost curves provided in sections 4 (CAPEX) and 5 (OPEX) of his work, a flexible cost model is developed that can be customized for different project specifications. Each curve is fitted to a power function of the form:

$$y = a \cdot x^b \tag{13}$$

This form was chosen because to avoid unrealistic behaviors at the lower end of the scale. Unlike polynomial fits, which can produce unrealistic negative costs, a power-law fit ensures a monotonic and physically meaningful cost relationship.

4 Design of Experiments

A preliminary DOE study provides valuable insights into the relative importance of design variables and relations between them and performance objectives. Additionally, DOE can help identify high-performance design configurations and establish general trends within the design space.

For this study, we use a Latin Hypercube sampling method with 508 samples to explore the design space. The designs corresponding to minimum and maximum LCOW are presented in Table 2.

To quantify the importance of each design variable, we employ feature importance analysis using a random forests regression model trained on the DOE dataset [33]. We compute feature importance using both mean decrease in impurity and permutation importance. These metrics indicate how much each variable contributes to predicting LCOW, helping identify potential reductions in design space complexity. The feature importance results are shown in Fig. 11.

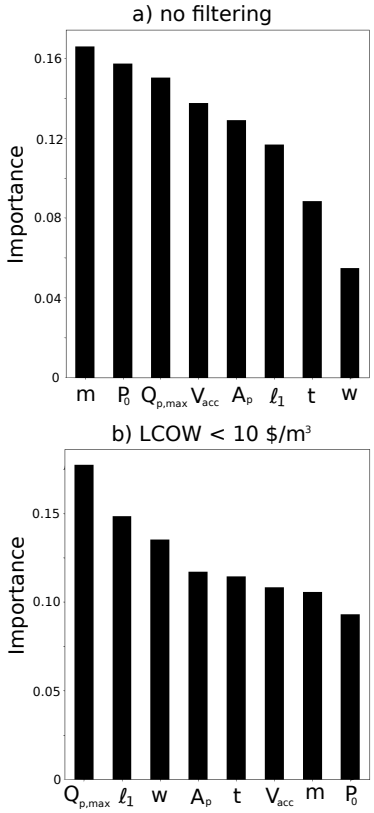

FIGURE 11: Feature Importance of Design Variables. a) shows the importance when using the full dataset, b) shows the importance when using a filtered dataset with only design with an LCOW $<$ 10 \$/m^3 included, 338 out of 508 designs met this criteria. This allows us to compare importance for creating reasonable designs (a) as well as making reasonable designs better (b).

5 Discussion

The DOE study reveals several key takeaways. The first takeaway is that the large disparity in LCOW values between the best and worst designs suggest substantial opportunities for optimization. The minimum LCOW case (2.29 \$/m^3) is orders of magnitude lower than the maximum LCOW case (7547 \$/m^3), emphasizing the importance of design space exploration and optimization.

The second takeaway is that poor system design can occur when WEC, PTO, and desalination plant capacities are mismatched. For example, the maximum LCOW case has a large WEC (24.5 m wide) and a large desalination plant capacity (9681 m^3/day), but an extremely small ℓ_1 value (0.276 m). A small ℓ_1 reduces the PTO's mechanical advantage, requiring excessive WEC motion to generate sufficient feedflow. A large WEC captures a high excitation torque from the waves and a

large desalination plant requires significant feedwater flow to be cost-effective, making larger ℓ_1 values essential.

Other inefficient configurations could arise such as a large WEC and large PTO paired with a small desalination plant, leading to excess feedwater being wasted through the pressure relief valve, or a large PTO and desalination plant with a small WEC which lacks the wave capture potential necessary to drive the system efficiently. These findings reinforce the necessity of a holistic model approach—optimizing only one subsystem (e.g., WEC, PTO, or desalination plant) in insolation is insufficient.

The third takeaway is that the minimum LCOW case suggests a departure from conventional design trends in the literature. Specifically, the minimum LCOW design features a smaller accumulator volume (1.51 m^3) and a larger desalination capacity (7467 m^3/day). In contrast, previous studies have favored larger accumulators to smooth flucations in feedwater flow. Yu and Jenne used accumulator volumes of 4 m^3 (2018) and 6 m^3 (2017) for a 3150 m^3/day plant [34, 11]. Brodersen et al. (2022) used a 6 m^3 accumulator for a 1700-2400 m^3/day desalination plant [35]. These studies assumed that large accumulators improve feedwater regulation, allowing smaller desalination plants to capture a higher percentage of the flow. While this logic holds when ignoring accumulator costs, the DOE suggests that reducing accumulator volume and increasing desalination plant capacity can lead to a lower LCOW, further reinforcing the need for a holistic model when designing a WDDS.

Beyond cost savings, a smaller accumulator may also enhance system performance. Michelén Ströfer et al. (2022) demonstrated that a negative-stiffness PTO improves energy transfer for electricity-generating WECs [7]. The accumulator acts as a spring, where larger volumes correspond to higher effective stiffness. Therefore, a smaller accumulator (i.e., lower positive stiffness) may enhance energy transfer efficiency in the WDDS PTO.

The feature importance results indicate that all design variables have contribute significantly to LCOW prediction, suggesting that reducing design space dimensionality is not advisable. However, WEC mass and accumulator pre-charge pressure appear more important for ensuring reasonable designs than for refining optimal designs. Their importance decreases in the filtered dataset (Fig. 11b), suggesting that while they influence feasibility, they are less critical for improving already viable designs. This suggests that their bounds could be tightened, restricting low-performance regions while preserving design flexibility in promising designs.

6 Conclusion

This study introduces an MDO framework for WDDS design. Preliminary DOE results suggest that MDO not only enhances system performance and but also influences conventional design trends. Notably, our findings suggest that reducing accumulator sizes and increasing SWRO plant capacities can yield lower LCOE, a departure from prior WDDS assumptions.

The insights gained from this study underscore the importance of holistic optimization, as poor subsystem coordination—such as mismatched WEC, PTO, and desalination capacities—can result in inefficient and costly designs. The feature importance analysis further highlights the key design parameters that influence performance, paving the way for targeted refinements in future optimization studies.

Future work should focus on:

1. Fully developing the PTO cost model by including piston and mechanism costs.
2. Adding control to the system dynamics model, with declutching control [36] identified as a particularly promising approach for WDDS.
3. Comparing MDO results to those obtained through traditional sequential design optimization.
4. Developing gradient-compatible models for the hydrodynamics and system dynamics modules to enable gradient-based optimization.
5. Investigating different WDDS PTO architectures, such as incorporating an ERU, within this framework.

The MDO framework presented in this study provides a systematic approach to optimizing WDDS, offering new pathways for improving desalination affordability and sustainability. Future advancements in control strategies, economic modeling, and real-world implementation will further strengthen the feasibility of wave-powered desalination as a scalable solution to global freshwater challenges.

REFERENCES

[1] Eliasson, J., 2015. "The rising pressure of global water shortages". *Nature,* ***517***(6), Jan.

[2] Li, Z., Siddiqi, A., Anadon, L. D., and Narayanamurti, V., 2018. "Towards sustainability in water-energy nexus: Ocean energy for seawater desalination". *Renewable and Sustainable Energy Reviews,* ***82***, Feb., pp. 3833–3847.

[3] Gillis, J., 2015. "California drought is made worseby global warming, scientists say". *New York Times*, Aug.

[4] of Energy, U. D., 2019. Powering the blue economy: Exploring opportunities for marine renewable energy in maritime markets, 4.

[5] Davies, P., 2005. "Wave-powered desalination: resource assessment and review of technology". *Desalination,* ***186***(1–3), Dec., pp. 97–109.

[6] Sobieszczanski-Sobieski, J., 1995. "Multidisciplinary design optimization: An emerging new engineering discipline". *Solid Mechanics and Its Applications*, p. 483–496.

[7] Ströfer, C. A. M., Gaebele, D. T., Coe, R. G., and Bacelli, G., 2023. "Control co-design of power take-off systems for

wave energy converters using wecopttool". *IEEE Transactions on Sustainable Energy,* ***14***(4), Oct., pp. 2157–2167.

[8] Peña-Sanchez, Y., García-Violini, D., and Ringwood, J. V., 2022. "Control co-design of power take-off parameters for wave energy systems". *IFAC-PapersOnLine,* ***55***(27), pp. 311–316.

[9] Rosati, M., and Ringwood, J. V., 2023. "Control co-design of power take-off and bypass valve for owc-based wave energy conversion systems". *Renewable Energy,* ***219***, Dec., p. 119523.

[10] Grasberger, J., Yang, L., Bacelli, G., and Zuo, L., 2024. "Control co-design and optimization of oscillating-surge wave energy converter". *Renewable Energy,* ***225***, May, p. 120234.

[11] Yu, Y.-H., and Jenne, D., 2018. "Numerical modeling and dynamic analysis of a wave-powered reverse-osmosis system". *Journal of Marine Science and Engineering,* ***6***(4), Nov., p. 132.

[12] Suchithra, R., Das, T. K., Rajagopalan, K., Chaudhuri, A., Ulm, N., Prabu, M., Samad, A., and Cross, P., 2022. "Numerical modelling and design of a small-scale wave-powered desalination system". *Ocean Engineering,* ***256***, July, p. 111419.

[13] Mi, J., Wu, X., Capper, J., Li, X., Shalaby, A., Wang, R., Lin, S., Hajj, M., and Zuo, L., 2023. "Experimental investigation of a reverse osmosis desalination system directly powered by wave energy". *Applied Energy,* ***343***, Aug., p. 121194.

[14] Simmons, J., 2024. "Modeling and design of hydraulic power take-offs for ocean wave-powered reverse osmosis desalination". PhD thesis, University of Minnesota, 4.

[15] Seader, J. D., Henley, E. J., and Roper, D. K., 2011. *SEPARATION PROCESS PRINCIPLES: Chemical and Biochemical Operations*, 3rd ed. Wiley.

[16] DuPont, 2024. Filmtec™ sw30hr-380 element product data sheet. Datasheet, Oct.

[17] Falnes, J., and Kurniawan, A., 2020. *Ocean Waves and Oscillating Systems: Linear Interactions Including Wave-Energy Extraction*, 2nd ed. Cambridge University Press.

[18] Ancellin, M., and Dias, F., 2019. "Capytaine: a Python-based linear potential flow solver". *Journal of Open Source Software,* ***4***(36), apr, p. 1341.

[19] Newman, J., and Lee, C.-H., 2002. "Boundary-element methods in offshore structure analysis". *Journal of Offshore Mechanics and Arctic Engineering,* ***124***, 05, p. 81.

[20] Wec-sim (wave energy converter simulator).

[21] LaBonte, A., O'Connor, P., Fitzpatrick, C., Hallett, K., and Li, Y., 2013. "Standardized cost and performance reporting for marineand hydrokinetic technologies". In 1st Marine Energy Technology Symposiumt.

[22] Y.-H. Yu, D. J., R. Thresher, A. Copping, S. G., and Hanna, L., 2015. Reference model 5 (rm5): Oscillating surge wave energy converter. Tech. Rep. Report, Jan.

[23] ReasonTek, 2025. Low pressure accuumulator quote, 03.

[24] Slocum, A. H., Haji, M. N., Trimble, A. Z., Ferrara, M., and Ghaemsaidi, S. J., 2016. "Integrated pumped hydro reverse osmosis systems". *Sustainable Energy Technologies and Assessments,* ***18***, Dec., pp. 80–99.

[25] Haefner, M. W., and Haji, M. N., 2023. "Integrated pumped hydro reverse osmosis system optimization featuring surrogate model development in reverse osmosis modeling". *Applied Energy,* ***352***, Dec., p. 121812.

[26] Huehmer, R., Gomez, J., Curl, J. M., and Moore, K., 2011. "Cost modeling of desalination systems". In International Desalination Association World Congress, International Desalination Association World Congress, International Desalination Association World Congress.

[27] Wittholz, M. K., O'Neill, B. K., Colby, C. B., and Lewis, D., 2008. "Estimating the cost of desalination plants using a cost database". *Desalination,* ***229***(1–3), Sept., pp. 10–20.

[28] Elkadeem, M. R., Kotb, K. M., Sharshir, S. W., Hamada, M. A., Kabeel, A. E., Gabr, I. K., Hassan, M. A., Worku, M. Y., Abido, M. A., Ullah, Z., Hasanien, H. M., and Selim, F. F., 2024. "Optimize and analyze a large-scale grid-tied solar pv-powered swro system for sustainable water-energy nexus". *Desalination,* ***579***, June, p. 117440.

[29] Gökçek, M., and Gökçek, O. B., 2016. "Technical and economic evaluation of freshwater production from a wind-powered small-scale seawater reverse osmosis system (wp-swro)". *Desalination,* ***381***(site.), Mar., pp. 47–57.

[30] Yu, Y.-H., and Jenne, D., 2017. "Analysis of a wave-powered, reverse-osmosis system and its economic availability in the united states". In International Conference on Ocean, Offshore and Arctic Engineering.

[31] Agency, I. A. E., 2013. "Deep 5 user manual".

[32] Voutchkov, N., 2019. *Desalination project cost estimating and management*. CRC Press.

[33] Rogers, J., and Gunn, S., 2006. "Identifying feature relevance using a random forest". In SLSFS 2005, C. Saunders et al., eds., Vol. 3940 of *LNCS*, Springer, p. 173–184.

[34] Yi-Hsiang Yu, D. J., 2017. "Analysis of a wave-powered, reverse-osmosis system and its economic availability in the united states". In Proceedings of the ASME 2017 36th International Conference on Ocean, Offshore and Arctic Engineering OMAE2017.

[35] Brodersen, K. M., Bywater, E. A., Lanter, A. M., Schennum, H. H., Furia, K. N., Sheth, M. K., Kiefer, N. S., Cafferty, B. K., Rao, A. K., Garcia, J. M., and Warsinger, D. M., 2022. "Direct-drive ocean wave-powered batch reverse osmosis". *Desalination,* ***523***, Feb., p. 115393.

[36] Ringwood, J. V., Bacelli, G., and Fusco, F., 2014. "Energy-maximizing control of wave-energy converters: The development of control system technology to optimize their operation". *IEEE Control Systems,* ***34***(5), Oct., pp. 30–55.

A Tables of Parameters

TABLE 3: General Parameters

Parameter	Value	Units
gravitational acceleration	9.81	m/s^2
ocean density	1025	kg/m^3
distance to shore	500	m
ocean temperature	298.15	K
water depth	12	m
wave direction	0	degrees
wave spectrum	Pierson–Moskowitz	-
significant wave height	2.64	m
peak period	9.86	s
Fixed Charge Rate	10.8	%

TABLE 4: SWRO Parameters

Parameter	Value	Units
feed flow total dissolved solids	40000	mg/L
permeate flow total dissolved solids	500	mg/L
salt molar weight	58.44	g/mol
water permeability coefficient	2.57×10^{-12}	m^3/N-s
recovery ratio	51.5	%
single unit membrane area	35	m^2
single unit permeate flow rate	24.6	m^3/day

TABLE 5: WEC Parameters

Parameter	Value	Units
draft	9	m
cg draft factor	-0.7778	-
unit inertia	14.57	m^2
RM5 surface area	1214	m^2
RM5 flap cost	3364648.63	$
RM5 base cost	1706415.27	$
RM5 bearings cost	17420.34	$
RM5 mooring cost	997819.2	$
RM5 monitoring cost	616480.27	$/yr
RM5 marine operations cost	101387.23	$/yr
RM5 shore operations cost	347280.29	$/yr
RM5 parts cost	86237.2	$/yr
RM5 consumables cost	17480.19	$/yr
RM5 insurance rate	2	%

TABLE 6: Mechanism Parameters

Parameter	Value	Units
ℓ_2	4.7	m
ℓ_3	0	m
max piston stroke	20	m

TABLE 7: Solver Parameters

Parameter	Value	Units
BEM frequencies	0.2, 0.34, 0.48, ..., 3	rad/s
SysDyn time step	0.1	s
SysDyn sim time	300	s